

1 **Enhanced coastal shoreline modelling using an Ensemble Kalman**
2 **Filter to include non-stationarity in future wave climates**

3
4 Raimundo Ibaceta¹, Kristen D. Splinter¹, Mitchell D. Harley¹ and Ian L. Turner¹

5
6 ¹Water Research Laboratory, School of Civil and Environmental Engineering UNSW Sydney,
7 NSW 2052, Australia.

8 Corresponding author: Raimundo Ibaceta (r.ibacetavega@unsw.edu.au)

9
10 Key Points

- 11
- 12 • A data-assimilation Dual State-Parameter Ensemble Kalman Filter (EnKF) methodology is
13 integrated within an established shoreline model
 - 14 • Non-stationary model parameters are obtained, with the accuracy and sampling frequency of
15 shoreline data critical to overall EnKF skill
 - 16 • Time-varying model parametrizations are physically linked to non-stationary wave forcing,
17 resulting in more accurate shoreline predictions
- 18

19 **Abstract**

20 A novel approach to improve seasonal to interannual sandy shoreline predictions is presented,
21 whereby model free parameters can vary in time, adjusting to potential non-stationarity in the
22 underlying model forcing. This is achieved by adopting a suitable data assimilation technique
23 (Dual State-Parameter Ensemble Kalman Filter) within the established shoreline evolution model
24 ShoreFor. The method is first tested and evaluated using synthetic scenarios, specifically
25 designed to emulate a broad range of natural sandy shoreline behavior. This approach is then
26 applied to a real-world shoreline dataset, revealing that time-varying model free parameters are
27 linked through physical processes to changing characteristics of the wave forcing. Greater
28 accuracy of shoreline predictions is achieved, compared to existing stationary modelling
29 approaches. It is anticipated that the wider application of this method can improve our
30 understanding and prediction of future beach erosion patterns and trends in a changing wave
31 climate.

32 **Plain Language Summary**

33 Understanding and predicting future changes along sandy coastlines worldwide is highly relevant
34 for coastal management in the context of climate change. In the future, the changing occurrence
35 of storms – and over longer timescales, rising sea levels - are expected to result in new patterns
36 of shoreline erosion. It is very common for shoreline change models to use past records of
37 measured shorelines and waves to match mathematical equations to these existing observations.
38 However, the validity of these types of shoreline models to predict the future is questionable,
39 when waves and storm patterns around the world in coming decades are expected to be different
40 to those observed in the past. A new methodology is presented to address this issue by exploring
41 how a mathematical shoreline model can self-adjust to wave climates that vary through time. The
42 proposed methodology is shown to be successful at improving shoreline predictions.

43

44 **1 Introduction**

45 Coastal managers have an increasing need for reliable tools that predict the response of sandy
46 coastlines worldwide to the impacts of extreme storm events, shifting regional wave climates and
47 rising sea levels. Semi-empirical shoreline models are proving to be increasingly successful at
48 predicting shoreline variability and evolution at seasonal to multiyear timescales (e.g., Splinter et
49 al., 2014; Yates et al., 2009). However, the complex spatio-temporal interactions of the different
50 processes driving shoreline change make multi-decadal predictions challenging (Montaño et al.,
51 2020), limiting our confidence in shoreline predictions at timescales extending to decades and
52 beyond (Ranasinghe, 2020).

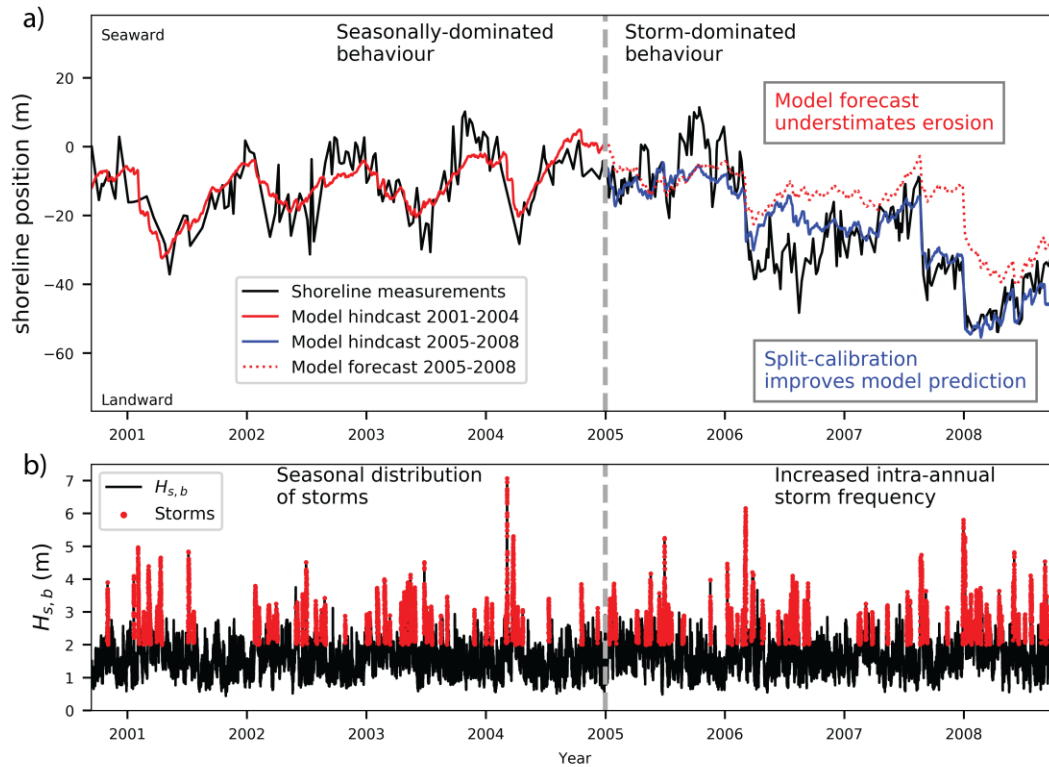
53

54 The present generation of shoreline models typically rely on a single period of past wave forcing
55 and observed shoreline measurements to establish the optimal magnitude of model free
56 parameters (e.g., Davidson et al., 2019; Long & Plant, 2012). It is then assumed that differences
57 between predicted and measured shorelines arise from further unresolved morphological
58 processes, inaccuracy in shoreline measurements and/or uncertainty in wave
59 modelling/measurements (Montaño et al., 2020). But crucially, by this approach it is implicitly
60 assumed that all model free parameters are stationary, even though the calibrated model may
61 then be used to explore past and future shoreline patterns and trends (e.g., Antolínez et al., 2019;
62 Vitousek et al., 2017). This use of a time-invariant approach to model free parameter estimation
63 necessarily introduces potential biases associated with the particular time period and/or duration
64 of the selected wave and shoreline dataset (D'Anna et al., 2020; Splinter et al., 2013) that is used
65 to perform the calibration. Recent work (D'Anna et al., 2020; Montaño et al., 2020) confirms
66 that shoreline hindcasting and forecasting is highly dependent on the selected calibration period.
67 In the context of a changing climate - and as a result, anticipated temporal variability in the key
68 wave and water-level drivers of shoreline evolution (Wong et al., 2014) - this assumption of
69 model free parameter stationarity must be further examined.

70

71 Other fields of geophysical research provide useful guidance on the implementation and physical
72 interpretation of non-stationary model parametrization. For example, Gove & Hollinger (2006)
73 applied a dual state-parameter Unscented Kalman Filter to explore the time evolution of model
74 parameters in problems of surface-atmosphere exchange, in which the observed changes were

75 linked to seasonal atmospheric-driven variability. More recently, hydrological applications have
76 examined the adjustment of rainfall-runoff parametrizations to improve model prediction
77 capabilities resulting from dynamic catchments (e.g., Grigg & Hughes, 2018; Pathiraja et al.,
78 2016a) and climate variability (e.g., Stephens et al., 2019; Xiong et al., 2019). Applied to
79 shoreline modelling, Splinter et al. (2017) used a simplified methodology of split-calibration
80 spanning two consecutive 4-year time periods at the Gold Coast, Australia. By this exploratory
81 approach, a substantial difference between the two time periods in one of the key model free
82 parameters (frequency response) was observed. This was found to be consistent with further
83 analysis that revealed a significant difference in the occurrence and distribution of storm wave
84 events between the two consecutive calibration periods. As illustrated in Figure 1, it was
85 observed that the shoreline response shifted from a distinctly seasonally-dominated mode
86 (annual cycle) to a more storm-dominated (~monthly) mode of behavior, highlighting the
87 challenge of assuming wave climate stationarity when applied to multi-year shoreline prediction
88 and forecasting.



89

90 **Figure 1.** (a) Modelled vs measured shoreline evolution; and (b) breaking significant wave
 91 height $H_{s,b}$ for an 8-year period at the Gold Coast, Australia, adapted from Splinter et al., (2017).
 92 The shoreline model was found to significantly underestimate the observed shoreline erosion
 93 from 2005 onwards when calibrated to the 4-year (2001-2004) period only. Subsequent analysis
 94 of the Gold Coast wave climate found that this time period coincided with a distinct shift from a
 95 seasonal wave climate towards increased intra-annual variability in storm frequency. A second
 96 calibration based on the 2005-2008 period only significantly improved model forecasts. Only by
 97 applying this ‘split calibration’ approach could reasonable hindcasts of shoreline behaviour
 98 spanning the full 8 years be achieved.

99 In a recent review of climate change-driven coastal erosion modelling, Toimil et al. (2020)
 100 concluded that uncertainty across all constituents of the modelling framework, including model
 101 parameters, should be considered. To achieve this objective, data assimilation techniques offer
 102 the potential to continuously adjust model parameters as additional state (i.e., shoreline)
 103 observations become available (Evensen, 2010). In the new work presented here, a novel
 104 methodology to enhance sandy shoreline modelling is developed, in which a suitable data
 105 assimilation technique is integrated within an established shoreline evolution model. A Dual
 106 State-Parameter Ensemble Kalman Filter (EnKF) (Pathiraja et al., 2016b) is adapted for this

107 purpose, and implemented within the generalized version of the cross-shore ShoreFor model
 108 (Splinter et al., 2014). The approach is first tested using synthetic wave climate scenarios,
 109 specifically designed to emulate a range of distinct and naturally occurring sandy shoreline
 110 behavior. The technique is then applied to a real-world observational dataset, where it is
 111 determined that the time-variation in model free parameters can be linked through physical
 112 processes to the changing characteristics of the wave forcing at this long-term study site.

113 2 Methods

114 2.1 Shoreline Model

115 ShoreFor (Davidson et al., 2013) is a semi-empirical model based on the behavioral concept that
 116 shorelines continuously evolve towards a time-varying equilibrium position. In the generalized
 117 form of this model (Splinter et al., 2014; hereafter SPLI14), the cross-shore rate of shoreline
 118 change (dx/dt) is given by:

$$119 \quad \frac{dx}{dt} = c^a F^a + c^e F^e + b \quad (1)$$

120 whereby the forcing term $F^{a,e} = P^{0.5} \Delta\Omega_{a,e} / \sigma_{\Delta\Omega}$ accounts for the wave power (P) and the
 121 disequilibrium dimensionless fall velocity ($\Delta\Omega$), which in turn dictates the potential direction
 122 either offshore ($\Delta\Omega_e$, when $\Delta\Omega < 0$) or onshore ($\Delta\Omega_a$, for $\Delta\Omega > 0$) of cross-shore sediment
 123 transport. Within this forcing term the disequilibrium component $\Delta\Omega = (\Omega_{eq} - \Omega)$ and its
 124 associated standard deviation $\sigma_{\Delta\Omega}$ are computed from the dimensionless fall velocity Ω at the
 125 break point (i.e., the seaward edge of the surf zone) and a time-varying equilibrium expression
 126 (after Wright et al., 1985) given by:

$$127 \quad \Omega_{eq} = \left[\sum_{i=1}^{2\phi} 10^{-i/\phi} \right]^{-1} \sum_{i=1}^{2\phi} \Omega_i 10^{-i/\phi} \quad (2)$$

128 Note that the additional term b in (1) simply accounts for any unresolved processes. Importantly,
 129 the model in Equation 1 includes three wave-driven cross-shore sediment transport-related
 130 parameters c^a , c^e and ϕ that require calibration. The magnitude rate parameters c^a and c^e (in
 131 $m^{1.5} s^{-1} W^{-0.5}$) are proxies for the accretion/erosion sediment transport efficiency and the
 132 frequency rate parameter ϕ (in days) represents a response time. Based on extensive testing of
 133 the ShoreFor model at a diverse range of seasonal and storm-dominated sandy coastlines in
 134 Australia, Europe and the USA, SPLI14 proposed generalized parametrizations for these rate

135 parameters based on the mean interannual ($\geq \sim 5$ years) $\bar{\Omega}$, consistent with well-established
136 relationships (e.g., Wright and Short, 1984) between modal beach states and cross-shore
137 processes. Conceptually, mild-slope beaches experience slower rates of shoreline changes (i.e.
138 $\phi > 100$ days) and decreased sediment exchange efficiency (lower c^a and c^e values) between
139 the surf zone and beach face. Conversely, the breaker line tends to be closer to the beach face at
140 steeper beaches, enhancing efficient (larger c^a and c^e magnitudes) and rapid (i.e. $\phi < 100$ days)
141 sediment exchange. Within this framework, Davidson et al., (2013) found that $\phi \cong 100$ days
142 usefully defines the approximate transition between storm-dominated and more seasonal
143 shoreline response. To calibrate the ShoreFor model for a specific time period, SPLI14 assumes
144 c^e is proportional to c^a and determines the remaining parameters via least-squares optimization
145 for pre-computed timeseries of $\Omega_{eq}(\phi)$ in the range of $\phi = 5$ to 1000 days. In the present work,
146 parameters are allowed to independently vary in time within the EnKF recursion (Section 2.3).
147 The reader is referred to Davidson et al., (2013) and SPLI14 for a complete description of the
148 model.

149 **2.2 Synthetic scenarios with the ShoreFor model**

150 Ten shoreline timeseries each spanning 20-years at 3-hourly sampling intervals were generated
151 using ShoreFor (Equation 1), forced by a set of synthetic wave records (See Figure S1,
152 Supporting Information) based on observations from three different sites characterizing seasonal
153 (e.g., Pacific North West - USA, Ruggiero et al., 2016), storm (e.g., Sydney - Australia, Short &
154 Trenaman, 1992) and mixed seasonal-storm wave climates (e.g., Gold Coast - Australia). It is
155 anticipated (see Figure S2b, Supporting Information) that model parameter variability may be
156 modulated at both multi-year ($O(5-10$ years)) and longer inter-decadal timescales, responding to
157 climate patterns (e.g. ENSO) as well as longer-term trends in wave climate (e.g., Young & Ribal,
158 2019). As is summarized in Figure 2a, four shape functions were developed to represent differing
159 modes of parameter variability and longer-term trends: simple time-invariant (Shape 1), a linear
160 negative trend (Shape 2), a sinusoidal function with a representative period of 10 years (Shape 3)
161 and a step-wise function (Shape 4). To generate the 10 synthetic scenarios, these four parameter
162 shapes and three different wave climates were then combined with increasing degrees of
163 complexity. A full description of this process is detailed in the accompanying Supporting
164 Information. As the focus here is on the non-stationarity of cross-shore wave-driven parameters,

165 for all ten scenarios the b term (see Equation 1) is omitted from the model. Figures S3–S5 in the
166 accompanying Supporting Information present the synthetic shoreline and parameter timeseries
167 for all 10 scenarios.

168 The resulting shoreline timeseries are then subsampled at time intervals (dt) of 1, 7, 15 and 30
169 days, representative of a range of typical sampling frequencies used for ongoing shoreline
170 monitoring programs worldwide (e.g., Holman & Stanley, 2007; Turner et al., 2016) and random
171 noise added ($\sim N(0, R^2)$, $R=1:1:12$ m) to characterize the accuracy of various shoreline
172 measurement methods that are typically used (see Harley et al., 2011). The final result is a total
173 of 480 individual test cases with known parameter non-stationarity.

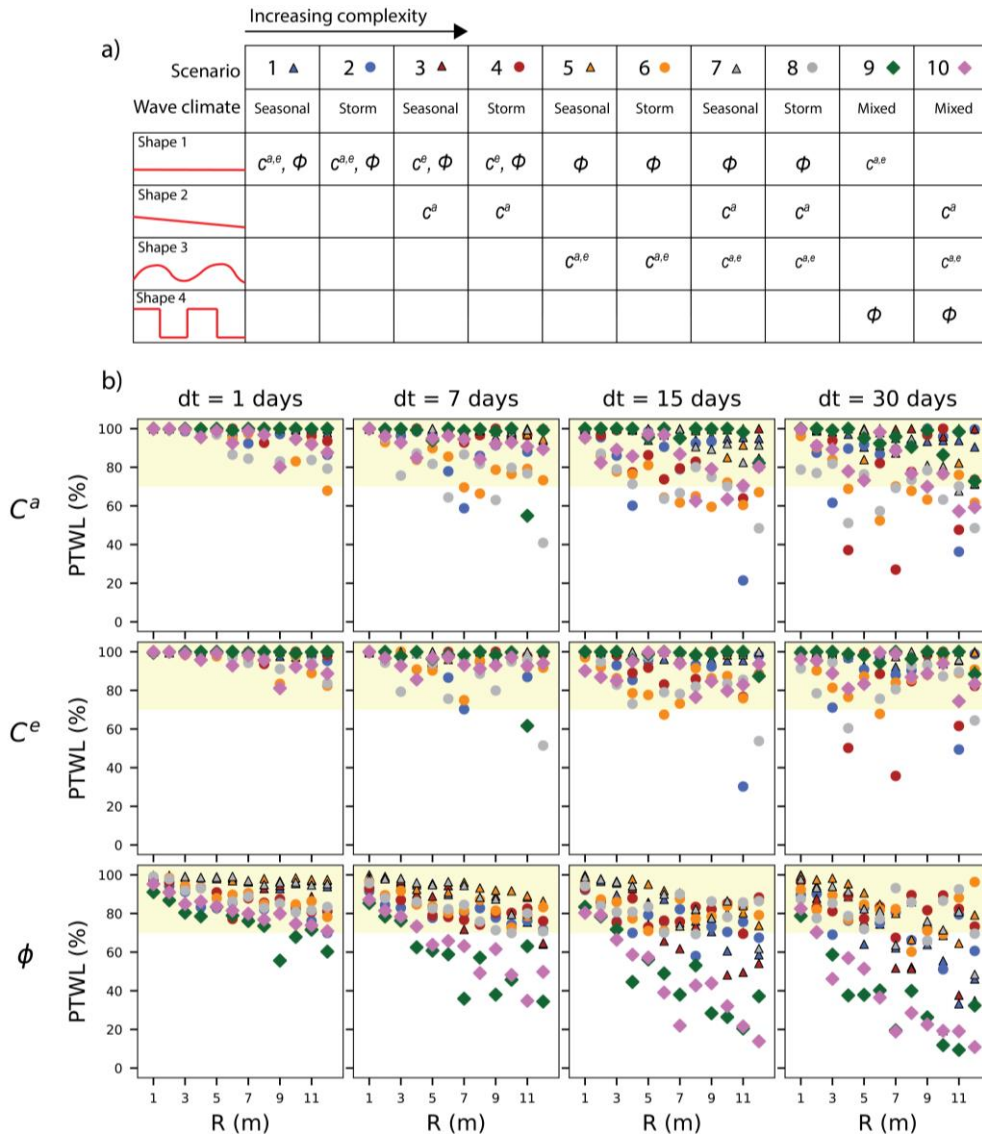
174 **2.3 Dual State-Parameter Ensemble Kalman Filter**

175 To explore parameter non-stationarity within the context of an established shoreline model, the
176 Dual State-Parameter EnKF algorithm proposed by Pathiraja et al., (2016b, 2016a) was
177 implemented. While it is possible to define a parameter evolution model within the EnKF, this
178 requires some *a priori* knowledge about the parameter non-stationarity (Pathiraja et al., 2016b).
179 Here it is assumed no information about temporal parameter variability is available so instead a
180 random-walk approach is applied.

181
182 The full details of the methodology are summarized in Figure S6 of the accompanying
183 Supporting Information. Briefly, for each EnKF experiment (i.e. model run) the method
184 initializes system states (i.e., shorelines) and model parameters as random variables created from
185 n ensemble members of known mean and error characteristics at $t=0$, and propagates these in
186 time as a Monte Carlo application of the well-known Kalman Filter (Evensen, 2010). At each 3-
187 hourly time-step, the shoreline model first uses inflated (i.e. process noise included) background
188 parameter ensembles modeled as a random-walk to estimate shorelines at the next time-step.
189 This continues until a new shoreline observation is available, which in turn is dependent on the
190 particular sampling frequency (dt). At this point, parameter ensembles are updated based on the
191 shoreline observation ensembles (i.e. mean with error statistics mirroring the measurement
192 accuracy, R in Section 2.2). These updated parameters are then used to provide new shoreline
193 estimates, which are then state-updated using the same observations of the parameter update
194 step. Importantly, Pathiraja et al., (2016b) found that the magnitude of parameter ensemble

195 inflation (process noise) added at each time step was critical to successfully track parameter
196 changes, otherwise updated estimates with lower variance than the previous time-step resulted in
197 nearly time-invariant parametrizations (e.g., Long & Plant, 2012; Vitousek et al., 2017). In the
198 present work, the approach of Xiong et al., (2019) was implemented, in which the magnitude of
199 process noise was sufficiently high to track time-varying parametrizations. Further details are
200 provided in the Supporting Information (S3).

201
202 Initial parameter ensembles are generated from truncated normal distributions to ensure that
203 parameters fall within their feasible range (Splinter et al., 2014). Rather than correcting for
204 erroneous initial parameter values, the purpose is to assess the EnKF performance for tracking
205 the potential non-stationarity of some or all model parameters. Therefore, the optimum initial
206 conditions with standard deviation spanning the range of values previously determined by
207 SPLI14 were implemented. The exceptions to this approach were for Scenarios 1 and 2, since
208 these cases are fully time-invariant, so instead random initial conditions sampled from a uniform
209 distribution were adopted. An analysis (see Supporting Information S4) for Scenario 10 using
210 different ensemble sizes ($n=10, 25, 50, 100, 250$ and 500) and number of experiments ($NE = 1,$
211 $10, 25$ and 50) showed that single experiments (i.e. $NE=1$) provide good EnKF skill at
212 sufficiently large ensemble-sizes ($n = 500$), necessary to minimize covariance inflation by under-
213 sampling (e.g. Keller et al., 2018). For the purposes of this work we adopt $NE=1$ and $n=500$.
214 Thus, a total of 480 individual experiments were used to explore the EnKF performance to
215 varying wave climate, shoreline measurement frequency and accuracy, and degrees of parameter
216 variability.



217

218 **Figure 2.** Ten synthetic shoreline scenarios generated with ShoreFor and sampled at a range
 219 of frequencies, incorporating increasingly complex combinations of parameter variability and
 220 a range of synthetic wave climates. (a) The four shape functions are: time-invariant (Shape
 221 1), a linear negative trend (Shape 2), a sinusoidal function with a representative period of 10
 222 years (Shape 3) and a step-wise function (Shape 4). As is tabulated, these are then applied in
 223 an increasingly complex combination of time-varying model parameters and either a
 224 seasonal, storm-driven or mixed seasonal-storm wave climate. For scenarios 7, 8 and 10, c^a
 225 is modulated by both sinusoidal and linear negative trend shapes. (b) EnKF skill expressed as
 226 the percentage of time within acceptable limits (PTWL), when applied at different sampling
 227 frequencies $dt = 1, 7, 15$ & 30 days. These results are summarised for the three ShoreFor
 228 wave-driven parameters c^a, c^e, ϕ (top to bottom) as a function of shoreline measurement
 229 accuracy R (horizontal axes). Note that higher PTWL values indicate superior algorithm
 230 performance. Triangles (circles) correspond to cases generated by the seasonal (storm)

231 dominated wave climate scenarios 1 - 8. Diamonds correspond to the mixed seasonal-storm
232 wave climates in scenarios 9 and 10.

233 **3 Results**

234 **3.1 Synthetic Cases**

235 The performance of the EnKF is summarized in Figure 2b for the three wave-dependent
236 parameters c^a , c^e , ϕ (from top to bottom), different shoreline time-sampling $dt = 1, 7, 15$ and
237 30 days (from left to right) and shoreline measurement accuracy $R = 1:1:12$ m (horizontal axes).
238 The percentage of time the ensemble mean is within acceptable limits (denoted PTWL, after
239 Pathiraja et al., 2016b) is used as the performance metric, such that PTWL values closer to
240 100% indicate higher skill. Acceptable limits are defined for time t as $\theta_t^* + \rho d_p$, where θ_t^* is the
241 true synthetic parameter magnitude, d_p is the feasible range of parameters magnitude (SPLI14)
242 and ρ is the 10% fraction. Following the same approach as Pathiraja et al. (2016b), a benchmark
243 of $PTWL \geq 70\%$ is selected here to define cases where the EnKF methodology could be
244 reasonably anticipated to succeed when applied to real-world datasets. Accordingly, 89% of the
245 cases fulfil this condition. In general, results indicate that the EnKF performance is highly
246 dependent on the quality of the observational data, whereby more frequently sampled and less-
247 noisy measured shorelines result in higher PTWL for the majority of scenarios.

248
249 To explore this general conclusion in further detail, representative results for the highest quality
250 shoreline data ($dt = 1$ day, $R = 1$ m) are shown in Figure 3a-d for increasingly complex Scenarios
251 4, 5, 9 and 10, respectively. From top to bottom, panels show the EnKF estimations (shown in
252 black) of shoreline timeseries as well as the parameters c^a, c^e and ϕ , compared to their true
253 synthetic values (red dashed lines). Time-invariant (Shape 1), negative trend (Shape 2),
254 sinusoidal (Shape 3) and step-wise parameter functions (Shape 4) are well estimated by the
255 EnKF for the full range of idealized seasonal, storm and mixed wave climates.

256
257 Examples of parameter estimation sensitivity to varying shoreline measurement accuracy ($R = 1,$
258 4, 8 and 12 m, $dt = 7$ days) and frequency ($dt = 1, 7, 15$ and 30 days, $R = 4$ m) are shown in
259 Figure 3e-f for the complex Scenario 10. As anticipated, EnKF performance decreases for higher
260 levels of R (e.g. ϕ , Figure 3e). With decreasing observational quality data, parameter

261 convergence is slower as the EnKF algorithm weights the model equations more than the
262 observations (e.g., Long & Plant, 2012; see also S2 in Supporting Information).

263

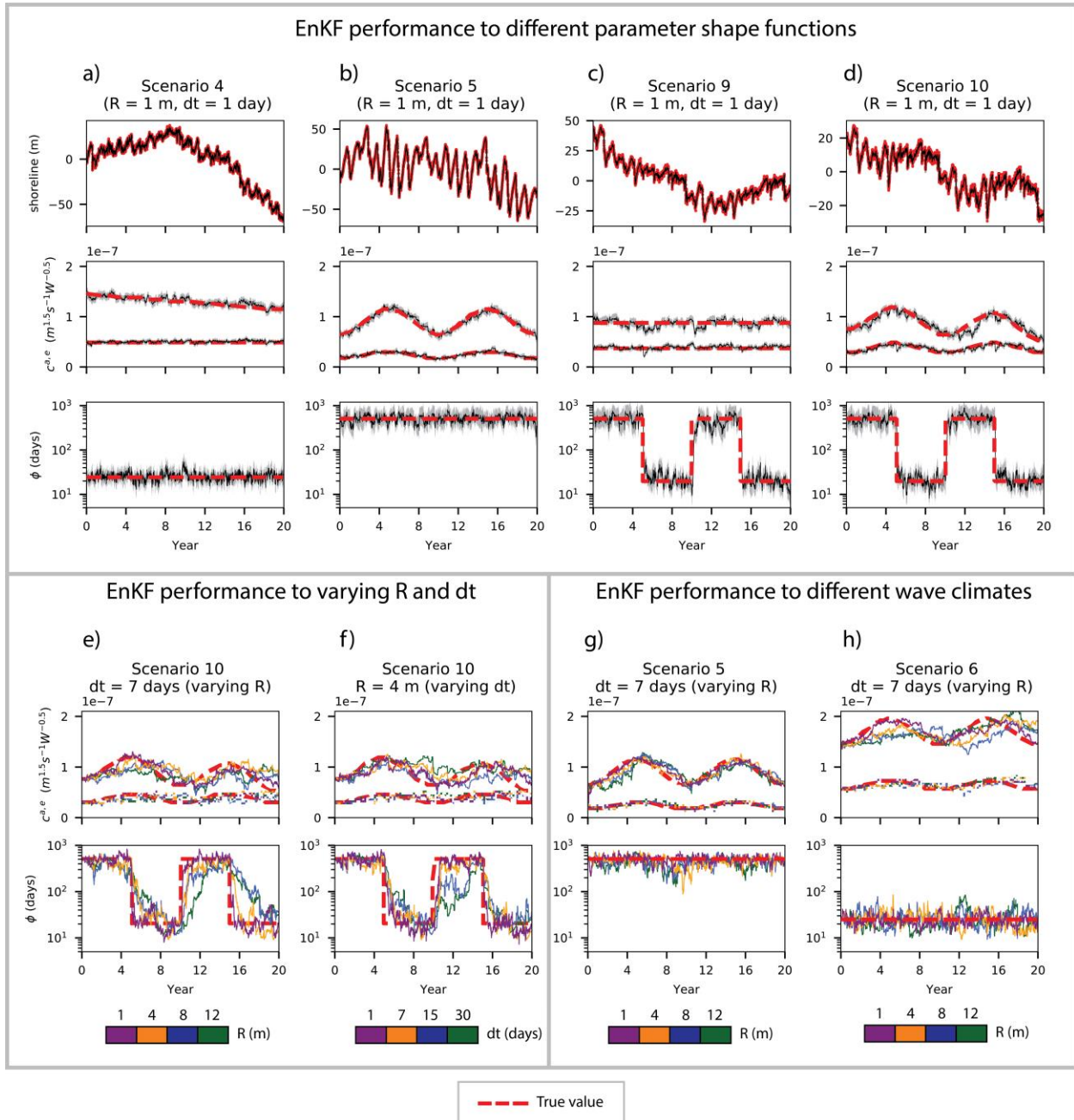
264 The effect of decreasing the frequency of shoreline observations (i.e. increasing dt) is also
265 apparent, resulting in less accurate and time-lagged parameter estimations (e.g. ϕ , Figure 3f).
266 However, Figure 2b demonstrates that results are more sensitive to observation accuracy (R)
267 rather than observation frequency (dt), with this being most pronounced for variations in ϕ
268 (lower panels). The time-lag between true and estimated parameters is assessed through the
269 convergence time of initially random sampled parameters at Scenarios 1 and 2 (fully time-
270 invariant). For all values of R and dt , 68% of the time-invariant cases (Figure 2, blue circles and
271 triangles) converge within 2 years (i.e. $PTWL > 90\%$). Notably, convergence and the ability to
272 capture time variability are inversely dependent on the level of process noise. For example,
273 adopting a lower process-noise (e.g., Long & Plant, 2012; Vitousek et al., 2017) results in 92%
274 of the time-invariant cases converging, however, this low level of noise severely limits the EnKF
275 performance on non-stationary parametrizations (Pathiraja et al., 2016b). It is therefore
276 concluded that the approach presented here is well suited to identifying and interpreting model
277 parameter non-stationarity using the established ShoreFor model at timescales down to
278 interannual. Notably, this convergence time is similar to Long and Plant (2012) who used an
279 Extended Kalman Filter applied to synthetic monthly-sampled shorelines of $R = 0.5$ m accuracy.
280 The new and more extensive analyses presented here provides the encouraging result that, for
281 shoreline measurement accuracy that can be more realistically obtained in the field (i.e., R up to
282 12 m) the EnKF performs well. Results for Scenarios 9 and 10 (Figure 2b) also indicate that ϕ
283 estimations are in general less accurate than those for c^a and c^e . This is because the time-varying
284 equilibrium expression given by Equation 2 is relatively insensitive for values of $\phi > 100$ days,
285 resulting in the potential for parameter equifinality and lower parameter estimation quality (e.g.,
286 Figure 3f, ~year 11).

287

288 The effect of differing wave climate characteristics can be also explored for varying levels of
289 shoreline measurement accuracy. Selecting a representative sampling interval of $dt = 7$ days and
290 comparing similar parameter combinations forced by the seasonally-dominated Scenario 5
291 (Figure 3g) versus the storm-dominated Scenario 6 (Figure 3h), results indicate an overall higher

292 skill level for the seasonal cases, up to and including the least-accurate shoreline data considered
 293 here ($R = 12$ m). This observation is attributed to the more frequent and rapidly varying
 294 characteristics of an episodic storm wave climate, compared to the more slowly evolving
 295 characteristics of a seasonal wave climate.

296



297
 298 **Figure 3.** Representative results of the EnKF algorithm. Examples for the highest quality
 299 shoreline data ($R = 1$ m and $dt = 1$ day) are shown in (a)-(b)-(c)-(d) (from top to bottom,
 300 shorelines, c^a , c^e and ϕ , note that $c^a > c^e$) for Scenarios 4, 5, 9 and 10, respectively. Black
 301 lines are the EnKF estimates, red dashed lines are the true synthetic values and grey bands

302 indicate uncertainty, represented by the standard deviation of the ensemble. Algorithm sensitivity
303 to dt and R is shown (Scenario 10) for (e) varying R (at $dt = 7$ days) and (f) varying dt (at $R = 4$
304 m). Depictive examples for algorithm sensitivity to wave climate characteristics are shown for
305 Scenarios 5 and 6 which are generated from (g) seasonal and (h) storm-dominated wave climate,
306 respectively. Note that parameter confidence bands in (e), (f), (g) and (h) were not included to
307 better facilitate visualization.

308

309 **3.2 Application to a real-world shoreline dataset**

310 The EnKF technique is now applied to a dataset of measured shorelines and waves at the Gold
311 Coast in southeast Australia spanning the 8-year period 2001-2008. This same shoreline dataset
312 was previously described in Splinter et al., (2017; hereafter SPLI17) and is also shown in Figure
313 1, being notable because of the observation that shoreline variability switched from a distinctly
314 seasonally-dominated mode to an episodic storm-dominated mode mid-way through the 8-year
315 measurement period. To obtain this dataset, 1 km alongshore-averaged shorelines were measured
316 on a weekly basis ($dt = 7$ days) using ARGUS video imagery (Holman & Stanley, 2007) with a
317 cross-shore accuracy of $R \sim 5$ m (Turner & Anderson, 2007). Wave buoy and shoreline
318 observations are assimilated into the ShoreFor model equations. As this is a real-world dataset, in
319 contrast to the synthetic cases (Section 3.1) the last term in Equation 1 is no longer fixed as $b =$
320 0 , to account for the possibility of secondary processes. However, it is anticipated that most of
321 the shoreline variability can be explained by cross-shore related parameters since minimal
322 alongshore-transport gradients have been suggested for this portion of coastline (e.g., Splinter et
323 al., 2011). The focus of the results presented here therefore remains on the primary wave-driven
324 cross-shore model parameters. To apply the new EnKF methodology, initial model parameter
325 estimates were obtained via the generalized parametrizations provided in SPLI14 applied to the
326 first 4-years of the wave record, along with an initial seed value of $b = 0$. To explore and
327 compare the new non-stationary EnKF results to the SPLI14 time-invariant calibration
328 methodology (Section 2.1), three additional ShoreFor model runs are presented: 1) a single
329 calibration spanning the full 8-year dataset; 2) split-sample calibration of the two consecutive
330 time-periods T1 (2001-2004) and T2 (2005-2008) as reported in SPLI17 (see Figure 1); and 3)
331 use of the stationary model free parameters derived for T1 to forecast the shoreline variability in
332 T2.

333

334 A summary of these results is presented in Figure 4. From top to bottom, Figure 4a shows the
335 shoreline predictions for the four different ShoreFor model outputs, along with Figure 4b-d the
336 corresponding values of non-stationary/stationary model free parameters c^a (continuous lines),
337 c^e (dashed lines), ϕ and b . As was previously observed in SPLI17, Figure 4 demonstrates that
338 shoreline and parameter estimation is sensitive to the selected calibration period, bringing into
339 question the validity of the assumption of stationarity. Encouragingly, comparison of the new
340 non-stationary EnKF approach (Figure 4a, black line) that now enables the model free
341 parameters to continuously evolve in time, can be seen to result in enhanced model skill (EnKF₈₋
342 _{year}, $\rho=0.95$, NMSE=0.10, RMSE=4.89 m) when compared to the stationary calibration (Figure
343 4a, magenta line) based on the 8-year dataset (ShoreFor_{8-year}, $\rho =0.82$, NMSE=0.33, RMSE=8.84
344 m). A similar improvement in error statistics results when comparing EnKF predictions to the
345 stationary-calibrations from individual T1/T2 periods (see Figure 4 caption for full details).

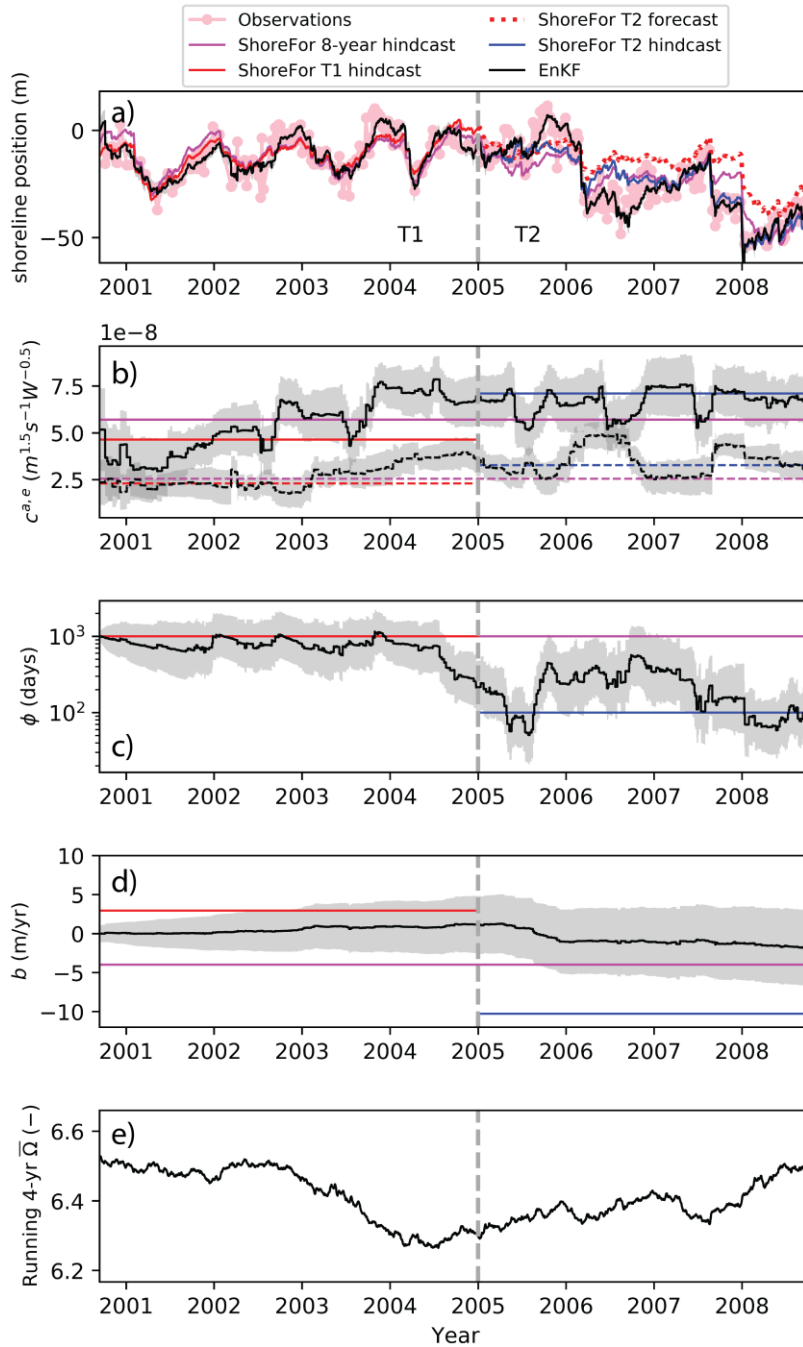
346

347 SPLI17 relied on subjective visual observation to distinguish the two time periods of T1 and T2
348 to undertake the reported split calibration. A key advantage of the new EnKF approach is that it
349 is able to continuously vary model parameters to best fit the shoreline observations. In particular,
350 after an initial period (2001-2003) of increasing magnitudes in c^a and c^e , the multi-year
351 variability of both parameters from 2004 onwards (Figure 4b, black lines) converges more
352 closely to the magnitudes obtained in the T2 stationary calibration. Both c^a and c^e also show
353 shorter-term variability (~seasonal) which remains unexplained and outside the scope of the
354 present work. These changes suggest a relationship of this variability in c^a and c^e and an
355 underlying change in the forcing wave climate that requires further investigation (See
356 Discussion). As was previously determined for the synthetic cases (Section 3.1), ϕ is the most
357 challenging parameter to estimate primarily because the model is relatively insensitive for $\phi >$
358 100 days (see Section 2.1). In the Gold Coast real-world application presented here (Figure 4c),
359 during the time period T1 the time-evolving ϕ remains large ($\phi \cong 1000$ days) and relatively
360 constant, corresponding to a more seasonally dominated mode of shoreline behavior. In contrast,
361 during the following T2 period this parameter can be seen to deviate and vary substantially from
362 this value, oscillating towards lower magnitudes ($\phi \cong 100$ days) that are more indicative of a
363 period of storm-dominated shoreline behavior. As was previously anticipated, the b term (Figure
364 4d, black line) shows minimal variability over the 8-year period within the EnKF, in which a

365 mild negative trend starting in 2005 can be attributed to further unresolved processes driving
366 shoreline erosion.

367

368 The final model realization depicted in Figure 4 shows the effect of transferring stationary model
369 free parameters calibrated from the initial time period T1 into the following T2, analogous to the
370 forecasting of future shoreline behavior (e.g., Davidson et al., 2013). Unlike the EnKF
371 continuous parameter adjustment, the time-invariant approach indicates that the T2 shoreline
372 forecast (Figure 4a, red dotted line) continues to track the general multi-year variability observed
373 during T1, but underestimates shorter-term erosive periods that are encountered during T2 (e.g.
374 2008). As anticipated, this result highlights the inherent weakness in the assumption of parameter
375 stationarity when semi-empirical shoreline models are applied to out-of-calibration shoreline
376 prediction.



379 **Figure 4.** EnKF application to a real observational shoreline dataset at the Gold Coast, Australia,
 380 and compared to 3 different time-invariant SPLI14 ShoreFor runs: 1) overall 8-year period
 381 (magenta lines); 2) split-sample calibration (after SPLI17) of two consecutive time-periods T1
 382 (2001-2004, red lines) and T2 (2005-2008, blue lines); and 3) T2 model forecast obtained from
 383 T1 model calibration (red dotted lines in panel a). From top to bottom a) Shoreline observations
 384 (pink dots), shoreline EnKF estimates (black line), T1 model hindcast (red continuous line), T2
 385 model hindcast (blue line), complete 8-year hindcast period (magenta line) and T2 forecast

386 obtained from T1 model calibration (red dotted line). b) c^a (continuous lines) and c^e (dashed
 387 lines) with line colours as described for panel (a). Note that horizontal lines represent time-
 388 invariant approaches. Similarly, panels (c) and (d) show the frequency rate parameter (ϕ) and the
 389 b term estimated with the EnKF and from time-invariant approaches. Grey bands indicate
 390 uncertainty, represented by the standard deviation of the ensemble. (e) Running mean (4-year)
 391 dimensionless fall velocity at the wave breaking position. The EnKF predictions result in the
 392 following improved error statistics:

393 EnKF_{8yr}: $\rho=0.95$ NMSE=0.10 RMSE=4.89 m ShoreFor_{8yr}: $\rho=0.82$ NMSE=0.33 RMSE=8.8 m
 394 EnKF_{T1}: $\rho=0.86$ NMSE=0.26 RMSE=4.91m ShoreFor_{T1}: $\rho=0.74$ NMSE=0.45 RMSE=6.44 m
 395 EnKF_{T2}: $\rho=0.95$ NMSE=0.09 RMSE=4.88 m ShoreFor_{T2}: $\rho=0.86$ NMSE=0.26 RMSE=8.15 m

396 **4 Discussion and Conclusions**

397 Analysis of 480 test cases, comprising ten synthetic shoreline timeseries derived from an
 398 increasingly complex mix of four distinct parameter functions, three wave climate characteristics
 399 and differing levels of observation accuracy and time-sampling (Section 2.2), confirms that the
 400 EnKF technique is suitable for tracking non-stationary parametrizations (PTWL \geq 70%) to
 401 predict the cross-shore movement of shorelines at multi-year timescales (Section 3.1).
 402 Exceptions to this general conclusion include cases where the observation shoreline data is either
 403 too noisy ($R > \sim 6$ m) or measured too infrequently ($dt > \sim 15$ days), with measurement accuracy
 404 and frequency become decreasingly important for beaches exposed to more seasonal compared
 405 to storm-dominated wave climates. The overall improvement in the ability to predict shoreline
 406 behavior using the EnKF is illustrated by the real-world application at the Gold Coast presented
 407 in Figure 4, where the use of time-varying parameters and their uncertainty result in higher
 408 accuracy shoreline predictions spanning the total 8-year observation period. A salient
 409 characteristic of the EnKF is that ensemble inflation by sufficiently high magnitudes of process
 410 noise (Section 2.3) allows for non-stationary parameter estimation. While previous Kalman Filter
 411 applications to shoreline modelling (Long & Plant, 2012; Vitousek et al., 2017) have relied on
 412 the assumption of low process noise to achieve time-invariant parameter convergence and
 413 uncertainty reduction, the new advancement here is that the EnKF approach continuously
 414 explores potential parameter changes as new observations become available (e.g. Gove &
 415 Hollinger, 2006). The adopted EnKF process noise also performs well over time-invariant cases
 416 (e.g. Fig 3a-c, c^e), confirming that any observed non-stationarity (e.g. Fig 4) reflects the
 417 continuous model adjustment to differing time-periods.

418

419 It is of interest to now briefly explore this parameter adjustment to the underlying morphological
420 processes that may be occurring at a coastal site. For example, the Gold Coast application in
421 Section 3.2 reveals time periods commencing in mid-2004 when the magnitude of ϕ shifted from
422 essentially constant to an overall decrease in magnitude and increase in variability (Figure 4c),
423 corresponding to the previously identified switch in the wave climate and resulting shoreline
424 behavior from seasonal to storm-dominated (SPLI17). In addition, the EnKF captures a
425 multiyear variability in c^a and c^e that roughly follows the magnitude changes between T1/T2
426 periods of stationary calibration, with an initial increasing trend (2001-2003), and then roughly
427 constant with some seasonal variability (2004-onwards). The previous stationary approach
428 detailed in SPLI14 dictates that different magnitudes of the accretionary rate term c^a are linked
429 to modal beach states, represented as a function of the mean dimensionless fall velocity ($\bar{\Omega}$) at a
430 site (Section 2.1), and then assumes that the erosive rate term c^e is simply proportional to c^a .
431 According to SPLI14 parametrizations, magnitude increases in c^a would necessarily implicate
432 negative trends in the multi-year $\bar{\Omega}$. This multiyear relationship between c^a and $\bar{\Omega}$, as well as the
433 assumed proportionality of c^a and c^e appears to be captured by the EnKF during the initial
434 2001-2003 period. However, in the latter half of the data (2005-2008) these two terms appear to
435 oscillate on a seasonal frequency but in opposite directions (e.g. 2006, Figure 4b), suggesting
436 that these short-lived parameter fluctuations appear as a consequence of unresolved processes in
437 the model. While this requires further fundamental physical-process investigation, it is of interest
438 to recall that c^a and c^e in the ShoreFor model encapsulate cross-shore sediment transport
439 efficiency (Section 2.1), so this temporal variability may be linked to unresolved processes
440 associated with nearshore morphology. For example, Ruessink et al., (2009) used video images
441 to observe the decay of an outer bar at this same site in early 2006. The resulting loss of a
442 ‘protective’ outer bar and the formation of a new bar close to the shoreline matches with
443 increased/reduced efficiency in erosive (c^e) and accretive (c^a) processes, respectively that have
444 been captured here by the EnKF.

445 |
446 Synthetic and real-world results presented here emphasize the need for shoreline model
447 structures that can adjust to potential changes in the underlying physical forcing. Results suggest
448 that the EnKF method is able to capture this variability when applied over long-term datasets
449 subjected to natural variability at interannual scales and beyond, and for which waves are the

450 driver of the observed and/or anticipated shorelines changes. The inclusion of time-varying
451 parametrizations (and their uncertainty) offers the opportunity to ensure consistency between
452 modelled coastal evolution drivers and the underlying physical processes (Toimil et al., 2020),
453 and now warrants the EnKF application as a method to explore parameter changes and
454 investigate strategies to improve shoreline models in view of climate variability. This is
455 motivated by the advent of newly available global-scale shoreline detection methods using
456 satellite remote sensing (e.g., Kelly & Gontz, 2019; Vos et al., 2019) and the increasing public
457 availability of high resolution long-term shoreline datasets (e.g., Ludka et al., 2019; Turner et al.,
458 2016). It is anticipated that the approach presented here will be useful for exploring cross-shore
459 parameter variability as a first step for training model parameters and empirically relating their
460 variability to natural changes in forcing (e.g. Splinter et al., 2014) to ensure model transferability
461 during forecast periods.

462

463 Shoreline models will benefit from a clearer understanding and inclusion of cross-shore model
464 parametrizations, ensemble-based wave forcing (e.g. Davidson et al., 2017) and also from the
465 inclusion of additional processes such as alongshore sediment transport and sea level rise (e.g.,
466 Robinet et al., 2018; Vitousek et al., 2017). The approach presented here offers the potential to
467 provide a robust structure to account for uncertainty across all constituents of the shoreline
468 modeling framework (Toimil et al., 2020) and to predict future shoreline change and trends in
469 the face of inter-decadal shifting waves (Morim et al., 2019) and intensified climate
470 teleconnections patterns (Barnard et al., 2015; Mentaschi et al., 2017), with the the end-goal of
471 achieving reliable multi-decadal shoreline projections.

472 **Acknowledgments and data availability**

473 Wave data from the Gold Coast was provided by Gold Coast City Council
474 (<https://www.data.qld.gov.au/dataset/coastal-data-system-waves-gold-coast>). Wave data for the
475 seasonal and storm-dominated scenarios was obtained from the CAWCR dataset
476 (<http://hdl.handle.net/102.100.100/137152?index=1>). ARGUS images from which shorelines
477 were derived are provided by the Water Research Laboratory, UNSW Australia
478 (<http://ci.wrl.unsw.edu.au/current-projects/northern-gold-coast-narrowneck-reef/archived-data/>)
479 with funding from Gold Coast City Council. Raimundo Ibaceta is funded by NSW
480 Environmental Trust Environmental Research Program (RD2015/0128), UNSW and CONICYT

481 (now ANID) Becas de Doctorado en el Extranjero – Becas Chile N72180087. We thank
 482 Maurizio D’Anna and Sean Vitousek for their constructive reviews that helped to improve this
 483 work. We also wish to acknowledge Sahani Pathiraja and Lucy Marshall for thier initial
 484 discussion and assistance with previous applications of EnKF, and Joseph Long for his ideas and
 485 discussions during earlier stages of this work.

486 **References**

- 487 Antolínez, J. A. A., Méndez, F. J., Anderson, D., Ruggiero, P., & Kaminsky, G. M. (2019).
 488 Predicting Climate- Driven Coastlines With a Simple and Efficient Multiscale Model.
 489 *Journal of Geophysical Research: Earth Surface*, *124*(6), 1596–1624.
 490 <https://doi.org/10.1029/2018JF004790>
- 491 Barnard, P. L., Short, A. D., Harley, M. D., Splinter, K. D., Vitousek, S., Turner, I. L., et al.
 492 (2015). Coastal vulnerability across the Pacific dominated by El Niño/Southern Oscillation.
 493 *Nature Geoscience*, *8*(10), 801–807. <https://doi.org/10.1038/ngeo2539>
- 494 D’Anna, M., Idier, D., Castelle, B., Le Cozannet, G., Rohmer, J., & Robinet, A. (2020). Impact
 495 of model free parameters and sea- level rise uncertainties on 20- years shoreline hindcast:
 496 the case of Truc Vert beach (SW France). *Earth Surface Processes and Landforms*.
 497 <https://doi.org/10.1002/esp.4854>
- 498 Davidson, M., Steele, E., & Saulter, A. (2019). Operational Forecasting of Coastal Resilience,
 499 1385–1399. https://doi.org/10.1142/9789811204487_0121
- 500 Davidson, M A, Splinter, K. D., & Turner, I. L. (2013). A simple equilibrium model for
 501 predicting shoreline change. *Coastal Engineering*, *73*, 191–202.
 502 <https://doi.org/10.1016/j.coastaleng.2012.11.002>
- 503 Davidson, Mark A, Turner, I. L., Splinter, K. D., & Harley, M. D. (2017). Annual prediction of
 504 shoreline erosion and subsequent recovery. *Coastal Engineering*, *130*, 14–25.
 505 <https://doi.org/10.1016/j.coastaleng.2017.09.008>
- 506 Evensen, G. (2010). *Data assimilation: The ensemble kalman filter*. *Data Assimilation: The*
 507 *Ensemble Kalman Filter*. <https://doi.org/10.1007/978-3-540-38301-7>
- 508 Gove, J. H., & Hollinger, D. Y. (2006). Application of a dual unscented Kalman filter for
 509 simultaneous state and parameter estimation in problems of surface-atmosphere exchange.
 510 *Journal of Geophysical Research Atmospheres*, *111*(8), 1–21.
 511 <https://doi.org/10.1029/2005JD006021>
- 512 Grigg, A. H., & Hughes, J. D. (2018). Nonstationarity driven by multidecadal change in
 513 catchment groundwater storage: A test of modifications to a common rainfall–run-off
 514 model. *Hydrological Processes*, *32*(24), 3675–3688. <https://doi.org/10.1002/hyp.13282>

- 515 Harley, M. D., Turner, I. L., Short, A. D., & Ranasinghe, R. (2011). Assessment and integration
516 of conventional, RTK-GPS and image-derived beach survey methods for daily to decadal
517 coastal monitoring. *Coastal Engineering*, 58(2), 194–205.
518 <https://doi.org/10.1016/j.coastaleng.2010.09.006>
- 519 Holman, R. A., & Stanley, J. (2007). The history and technical capabilities of Argus. *Coastal*
520 *Engineering*, 54(6–7), 477–491. <https://doi.org/10.1016/j.coastaleng.2007.01.003>
- 521 Keller, J., Hendricks Franssen, H. J., & Marquart, G. (2018). Comparing Seven Variants of the
522 Ensemble Kalman Filter: How Many Synthetic Experiments Are Needed? *Water Resources*
523 *Research*, 54(9), 6299–6318. <https://doi.org/10.1029/2018WR023374>
- 524 Kelly, J. T., & Gontz, A. M. (2019). Rapid Assessment of Shoreline Changes Induced by
525 Tropical Cyclone Oma Using CubeSat Imagery in Southeast Queensland, Australia. *Journal*
526 *of Coastal Research*, 36(1), 72. <https://doi.org/10.2112/jcoastres-d-19-00055.1>
- 527 Long, J. W., & Plant, N. G. (2012). Extended Kalman Filter framework for forecasting shoreline
528 evolution. *Geophysical Research Letters*, 39(13), n/a–n/a.
529 <https://doi.org/10.1029/2012GL052180>
- 530 Ludka, B. C., Guza, R. T., O'Reilly, W. C., Merrifield, M. A., Flick, R. E., Bak, A. S., et al.
531 (2019). Sixteen years of bathymetry and waves at San Diego beaches. *Scientific Data*, 6(1),
532 161. <https://doi.org/10.1038/s41597-019-0167-6>
- 533 Mentaschi, L., Vousdoukas, M. I., Dosio, A., Voukouvalas, E., & Feyen, L. (2017). Global
534 changes of extreme coastal wave energy fluxes triggered by intensified teleconnection
535 patterns. *Geophysical Research Letters*, 2416–2426. <https://doi.org/10.1002/2016gl072488>
- 536 Montaña, J., Coco, G., Antolínez, J. A. A., Beuzen, T., Bryan, K. R., Cagigal, L., et al. (2020).
537 Blind testing of shoreline evolution models, 1–10. <https://doi.org/10.1038/s41598-020-59018-y>
- 539 Morim, J., Hemer, M., Wang, X. L., Cartwright, N., Trenham, C., Semedo, A., et al. (2019).
540 Robustness and uncertainties in global multivariate wind-wave climate projections. *Nature*
541 *Climate Change*, 9(9), 711–718. <https://doi.org/10.1038/s41558-019-0542-5>
- 542 Pathiraja, S., Marshall, L., Sharma, A., & Moradkhani, H. (2016a). Detecting non-stationary
543 hydrologic model parameters in a paired catchment system using data assimilation.
544 *Advances in Water Resources*, 94, 103–119.
545 <https://doi.org/10.1016/j.advwatres.2016.04.021>
- 546 Pathiraja, S., Marshall, L., Sharma, A., & Moradkhani, H. (2016b). Hydrologic modeling in
547 dynamic catchments: A data assimilation approach. *Water Resources Research*, 52(5),
548 3350–3372. <https://doi.org/10.1002/2015WR017192>
- 549 Ranasinghe, R. (2020). On the need for a new generation of coastal change models for the 21 st
550 century. *Scientific Reports*, 1–6. <https://doi.org/10.1038/s41598-020-58376-x>

- 551 Robinet, A., Idier, D., Castelle, B., & Marieu, V. (2018). A reduced-complexity shoreline change
 552 model combining longshore and cross-shore processes: the LX-Shore model. *Environmental*
 553 *Modelling and Software*. <https://doi.org/10.1016/j.envsoft.2018.08.010>
- 554 Ruessink, B. G., Pape, L., & Turner, I. L. (2009). Daily to interannual cross-shore sandbar
 555 migration: Observations from a multiple sandbar system. *Continental Shelf Research*,
 556 29(14), 1663–1677. <https://doi.org/10.1016/j.csr.2009.05.011>
- 557 Ruggiero, P., Kaminsky, G. M., Gelfenbaum, G., & Cohn, N. (2016). Morphodynamics of
 558 prograding beaches: A synthesis of seasonal- to century-scale observations of the Columbia
 559 River littoral cell. *Marine Geology*, 376, 51–68.
 560 <https://doi.org/10.1016/j.margeo.2016.03.012>
- 561 Short, A. D., & Trenaman, N. L. (1992). Wave climate of the sydney region, an energetic and
 562 highly variable ocean wave regime. *Marine and Freshwater Research*, 43(4), 765–791.
 563 <https://doi.org/10.1071/MF9920765>
- 564 Splinter, K. D., Strauss, D. R., & Tomlinson, R. B. (2011). Assessment of post-storm recovery of
 565 beaches using video imaging techniques: A case study at Gold Coast, Australia. *IEEE*
 566 *Transactions on Geoscience and Remote Sensing*, 49(12 PART 1), 4704–4716.
 567 <https://doi.org/10.1109/TGRS.2011.2136351>
- 568 Splinter, K. D., Turner, I. L., & Davidson, M. A. (2013). How much data is enough? The
 569 importance of morphological sampling interval and duration for calibration of empirical
 570 shoreline models. *Coastal Engineering*, 77, 14–27.
 571 <https://doi.org/https://doi.org/10.1016/j.coastaleng.2013.02.009>
- 572 Splinter, K. D., Turner, I. L., Davidson, M. A., Barnard, P., Castelle, B., & Oltman-Shay, J.
 573 (2014). A generalized equilibrium model for predicting daily to inter-annual shoreline
 574 response. *Journal of Geophysical Research: Earth Surface*, 119, 1936–1958.
 575 <https://doi.org/10.1002/2014JF003106>
- 576 Splinter, K. D., Turner, I. L., Reinhardt, M., & Ruessink, G. (2017). Rapid adjustment of
 577 shoreline behavior to changing seasonality of storms: observations and modelling at an
 578 open-coast beach. *Earth Surface Processes and Landforms*, 42(8), 1186–1194.
 579 <https://doi.org/10.1002/esp.4088>
- 580 Stephens, C. M., Marshall, L. A., & Johnson, F. M. (2019). Investigating strategies to improve
 581 hydrologic model performance in a changing climate. *Journal of Hydrology*,
 582 579(September), 124219. <https://doi.org/10.1016/j.jhydrol.2019.124219>
- 583 Toimil, A., Camus, P., Losada, I. J., Cozannet, G. Le, Nicholls, R. J., Idier, D., & Maspataud, A.
 584 (2020). Climate change-driven coastal erosion modelling in temperate sandy beaches:
 585 Methods and uncertainty treatment. *Earth-Science Reviews*, 103110.
 586 <https://doi.org/https://doi.org/10.1016/j.earscirev.2020.103110>
- 587 Turner, I. L., & Anderson, D. J. (2007). Web-based and “real-time” beach management system.
 588 *Coastal Engineering*, 54(6–7), 555–565. <https://doi.org/10.1016/j.coastaleng.2007.01.002>

- 589 Turner, I. L., Harley, M. D., Short, A. D., Simmons, J. A., Bracs, M. A., Phillips, M. S., &
590 Splinter, K. D. (2016). A multi-decade dataset of monthly beach profile surveys and inshore
591 wave forcing at Narrabeen, Australia. *Scientific Data*, 3, 1–13.
592 <https://doi.org/10.1038/sdata.2016.24>
- 593 Vitousek, S., Barnard, P. L., Limber, P., Erikson, L., & Cole, B. (2017). A model integrating
594 longshore and cross-shore processes for predicting long-term shoreline response to climate
595 change. *Journal of Geophysical Research: Earth Surface*, 122(4), 782–806.
596 <https://doi.org/10.1002/2016JF004065>
- 597 Vos, K., Splinter, K. D., Harley, M. D., Simmons, J. A., & Turner, I. L. (2018). Capturing intra-
598 annual to multi-decadal shoreline variability from publicly available satellite imagery.
599 *Coastal Engineering, in review*. <https://doi.org/10.1016/j.coastaleng.2019.04.004>
- 600 Vos, Kilian, Splinter, K. D., Harley, M. D., Simmons, J. A., & Turner, I. L. (2019). CoastSat: A
601 Google Earth Engine-enabled Python toolkit to extract shorelines from publicly available
602 satellite imagery. *Environmental Modelling and Software*, 122.
603 <https://doi.org/10.1016/j.envsoft.2019.104528>
- 604 Vos, Kilian, Harley, M. D., Splinter, K. D., Simmons, J. A., & Turner, I. L. (2019). Sub-annual
605 to multi-decadal shoreline variability from publicly available satellite imagery. *Coastal*
606 *Engineering*, 150(February), 160–174. <https://doi.org/10.1016/j.coastaleng.2019.04.004>
- 607 Wong, P. P., Losada, I. J., Gattuso, J. P., Hinkel, J., A, K., McInnes, K. L., et al. (2014). Coastal
608 Systems and Low-Lying Areas. In Intergovernmental Panel on Climate Change (Ed.),
609 *Climate Change 2014 – Impacts, Adaptation and Vulnerability: Part A: Global and*
610 *Sectoral Aspects: Working Group II Contribution to the IPCC Fifth Assessment Report:*
611 *Volume 1: Global and Sectoral Aspects* (Vol. 1, pp. 361–410). Cambridge: Cambridge
612 University Press. [https://doi.org/DOI: 10.1017/CBO9781107415379.010](https://doi.org/DOI:10.1017/CBO9781107415379.010)
- 613 Wright, L. D., & Short, A. D. (1984). Morphodynamic variability of surf zones and beaches: A
614 synthesis. *Marine Geology*, 56(1–4), 93–118. [https://doi.org/10.1016/0025-3227\(84\)90008-](https://doi.org/10.1016/0025-3227(84)90008-2)
615 2
- 616 Wright, L. D., Short, A. D., & Green, M. O. (1985). Short-term changes in the morphodynamic
617 states of beaches and surf zones: An empirical predictive model. *Marine Geology*, 62(3–4),
618 339–364. [https://doi.org/10.1016/0025-3227\(85\)90123-9](https://doi.org/10.1016/0025-3227(85)90123-9)
- 619 Xiong, M., Liu, P., Cheng, L., Deng, C., Gui, Z., Zhang, X., & Liu, Y. (2019). Identifying time-
620 varying hydrological model parameters to improve simulation efficiency by the ensemble
621 Kalman filter: A joint assimilation of streamflow and actual evapotranspiration. *Journal of*
622 *Hydrology*, 568(November 2018), 758–768. <https://doi.org/10.1016/j.jhydrol.2018.11.038>
- 623 Yates, M. L., Guza, R. T., & O'Reilly, W. C. (2009). Equilibrium shoreline response:
624 Observations and modeling. *Journal of Geophysical Research: Oceans*, 114(9).
625 <https://doi.org/10.1029/2009JC005359>
- 626 Young, I. R., & Ribal, A. (2019). Multiplatform evaluation of global trends in wind speed and

627 wave height. *Science*, 552(May), 548–552. <https://doi.org/10.1126/science.aav9527>

628 **Additional References of the Supporting Information**

629 Durrant, T., Greenslade, D., Hemer, M., & Trenham, C. (2014). *The Centre for Australian*
630 *Weather and Climate Research A partnership between CSIRO and the Bureau of*
631 *Meteorology A Global Wave Hindcast focussed on the Central and South Pacific*. Retrieved
632 from
633 <http://citeseerx.ist.psu.edu/viewdoc/download?doi=10.1.1.641.1743&rep=rep1&type=pdf>

634